Available online at www.sciencedirect.com

SCIENCE DIRECT®

Earth and Planetary Science Letters 228 (2004) 495–509

EPSL

www.elsevier.com/locate/epsl

Sulfur isotope partitioning during experimental formation of pyrite via the polysulfide and hydrogen sulfide pathways: implications for the interpretation of sedimentary and hydrothermal pyrite isotope records

Ian B. Butler[a,*], Michael E. Böttcher[b], David Rickard[a], Anthony Oldroyd[a]

[a] *Cardiff Sulfide Research Group, School of Earth, Ocean and Planetary Sciences, Cardiff University, Park Place, Cardiff CF10 3YE, UK*
[b] *Max Plank Institute for Marine Microbiology, Department of Biogeochemistry, Celsiusstr. 1, D-28359 Bremen, Germany*

Received 10 June 2004; received in revised form 18 August 2004; accepted 7 October 2004

Editor: B. Wood

Abstract

We show that the sulfur isotopic composition of sedimentary and hydrothermal pyrite is a good approximation of the average sulfur isotopic composition of the dissolved sulfide sources from which the pyrite formed. Consequently, pyrite sulfur isotope systematics normally provide little evidence of the pyrite-forming mechanism in most natural systems. Stable sulfur isotope partitioning during pyrite (FeS_2) synthesis via the polysulfide and H_2S pathways was investigated between 80 and 120 °C. Iron monosulfide (FeS) was reacted with hydrogen sulfide (H_2S) or tetrasulfide (S_4^{2-}) in aqueous solution under strictly anoxic conditions. The results provide independent confirmation of the hydrogen sulfide and polysulfide mechanisms. The measured isotopic composition of the synthesized pyrite is compared with (1) isotopic mixing models of the reactant reservoirs and (2) predictions based on the suggested mechanisms for the hydrogen sulfide and polysulfide pathways for pyrite formation. The isotopic composition of the pyrite product is consistent with the result predicted from the reaction mechanisms. Pyrite produced via the H_2S pathway has a composition reflecting isotopic contributions from both FeS and H_2S reservoirs. Pyrite formed via the polysulfide pathway inherits an isotopic composition dominated by the polysulfide reservoir. In both cases, solubility driven isotope exchange between FeS and aqueous S species contribute to the final pyrite composition. We show that published experimental sulfur isotope data for pyrite formation which apparently support conflicting pyrite-forming pathways, are consistent with pyritization via the polysulfide and H_2S pathways. Formation rates of natural pyrite, however, may be too slow compared to solubility exchange for the influence of the reaction pathway on the isotopic composition to be significant.

Keywords: pyrite; sulfur isotopes; reaction pathways; iron monosulfide; hydrogen sulfide; polysulfide

* Corresponding author. Tel.: +44 2920 875801; fax: +44 2920 874326.
E-mail address: Butler@earth.cf.ac.uk (I.B. Butler).

0012-821X/$ - see front matter © 2004 Elsevier B.V. All rights reserved.
doi:10.1016/j.epsl.2004.10.005

1. Introduction

The sulfur isotopic composition of pyrite is used as a major probe for investigating the evolution of ancient biogeochemical cycles and hydrothermal processes. Stable isotope studies of modern reduced sedimentary sulfur have focused on the sulfur isotopic composition of iron sulfide minerals [1–4]. In the sedimentary sulfur cycle, isotope fractionation is caused by dissimilative sulfate-reducing bacteria [5–7] with contributions from bacterial and chemical sulfide oxidation [5,8] and bacterial disproportionation of intermediate sulfur species [9–12]. Studies of recent hydrothermal sulfide mineralization utilize the sulfur isotope composition of metal sulfides to understand fluid mixing during mineralization [13–15]. In sea-floor hydrothermal environments, the isotopic composition of metal sulfides is a mixture of Mid-Ocean Ridge Basalt derived sulfur ($\delta^{34}S \approx 0‰$ [16]) and thermochemically reduced seawater sulfate ($\delta^{34}S \approx +21‰$ [17,18]). The principle contributions to the sulfur isotope composition of pyrite in sediments and hydrothermal environments are well understood. Less clear is how and if reactions involved in pyrite formation cause additional isotope partitioning.

1.1. Pyrite formation pathways

The initial condensed phase produced by the reaction of Fe with S(-II) in aqueous solutions is nanoparticulate (2–7 nm) mackinawite [19], which has been referred to as "amorphous FeS", "precipitated FeS" or "disordered mackinawite", but which we refer to as FeS. Several pathways for the reaction of FeS to FeS_2 have been proposed; however, stoichiometry, kinetics and mechanism have been determined only for the polysulfide [20,21] and H_2S [22,23] pathways. The polysulfide pathway involves the reaction of FeS and $S^{2-}_{n(aq)}$. The reaction is:

$$FeS_{(s)} \rightarrow FeS_{(aq)} + S^{2-}_{n(aq)} = FeS_{2(aq)} + S^{2-}_{n-1(aq)}. \quad (1)$$

The kinetics of the process are consistent with a mechanism involving the dissolution of FeS and reaction with aqueous polysulfide to form pyrite [20,21].

The H_2S pathway, initially observed as the reaction of pyrrhotite ($Fe_{1-x}S$) with $H_2S_{(aq)}$, was first described at temperatures exceeding 100 °C [24,25]. The reaction of FeS is rapid at ambient temperatures [22] and the reaction is:

$$FeS_{(s)} \rightarrow FeS_{(aq)} + H_2S_{(aq)} = FeS_{2(s)} + H_{2(g)}. \quad (2)$$

Kinetic data and product textures are consistent with a mechanism involving FeS dissolution before reaction with H_2S [23]. It is $H_2S_{(aq)}$, not $HS^-_{(aq)}$, which participates in the reaction mechanism; consequently, the rate is pH dependent and favoured in near neutral to slightly acidic conditions.

Other proposed mechanisms are based on phenomenological data but without complete determination of stoichiometry. These include the solid-state reaction of FeS and S° [26,27]:

$$FeS_{(s)} + nS^\circ_{(s)} = FeS_{2(s)} + n - 1S^\circ_{(s)}. \quad (3)$$

While Eq. (3) describes the net reaction, this solid phase process is unlikely at ambient temperatures. The mechanism of the observed reaction with S° may proceed via the polysulfide pathway [20,28]. The pyritization of FeS with sulfidic reactants in the presence of O_2 has been suggested to proceed via oxidative Fe-loss [29,30]:

$$2FeS_{(s)} + 2H^+_{(aq)} = FeS_{2(s)} + Fe^{2+}_{(aq)} + H_{2(g)}. \quad (4)$$

This conclusion was supported by sulfur isotope data, which showed that FeS_2 inherits the isotopic composition of the FeS [29].

In this contribution, we report the results of an investigation of the polysulfide and H_2S pathways using isotopically characterised reactants and test the veracity of proposed reaction mechanisms. We re-examine published sulfur isotope data [26,29] and reconcile apparently conflicting models for pyrite formation. Finally, we consider natural pyrite forming pathways and the application of our results for isotopic studies of pyrite formation.

2. Materials and methods

Pyrite synthesis utilized batch synthesis methods [22] and reactants (FeS, H_2S and Na_2S_4) of known sulfur isotope composition. All reagents were analytical grade and solutions were prepared with 18 MΩ cm water. Solutions were sparged with flowing O_2-

free grade N_2 [31] and reactions were prepared with N_2 purified using Zr at >350 °C [22].

2.1. Reactants

Two methods were used to prepare FeS. Method A: 100 ml each of 0.6 M $Na_2S \cdot 9H_2O$ and $(NH_4)_2Fe(SO_4)_2 \cdot 6H_2O$ solutions were mixed, filtered under N_2, washed and freeze-dried. Method B: 99% H_2S gas was bubbled through 100 ml of 0.6 M NaOH until saturated. FeS was precipitated by addition of 100 ml of 0.6 M $(NH_4)_2Fe(SO_4)_2 \cdot 6H_2O$ and filtered under N_2, washed and freeze-dried. FeS produced by method B was ^{34}S enriched over that produced by method A by 8‰.

Two H_2S sources were utilized. Pure (99%) $H_2S_{(g)}$ was added directly to the reaction vessel. Otherwise $H_2S_{(g)}$ was generated by acid decomposition of $Na_2S \cdot 9H_2O$ using 50% v/v H_2SO_4 and added to the reaction vessel. Sodium tetrasulfide, Na_2S_4, was prepared as a pure solid by fusion of stoichiometric mixtures of anhydrous Na_2S and S° [21,32].

2.2. Experimental procedure

Freeze-dried FeS was weighed into 120-ml glass ampoules in an N_2-flushed glove box with 10 ml of pH 6 buffer (0.02 M phosphate) and 1 ml of Ti(III) citrate [22,33] and the vessel was attached to a gas transfer manifold [22] and purged with N_2. H_2S was then added to the reaction vessel. Immediately after gas transfer the vessel was sealed off from the manifold and excess H_2S pumped to waste. The pressure in the ampoule was adjusted to 10–20 mbar below ambient pressure with N_2 and ampoule was hermetically sealed using a glassblower's torch. Sealed vessels were maintained at reaction temperature in a reaction oven with continual mixing. For experiments with tetrasulfide, Na_2S_4 was weighed into the ampoule with FeS and 20 ml of pH 8 buffer (0.02 M borate) was used. No H_2S was added to tetrasulfide experiments.

Repeatable H_2S transfer to the reaction vessel was essential. Several methods were investigated using procedural blanks and collection of H_2S as Ag_2S using excess 10% w/v $AgNO_3$ solution. Simple transfer using advective and diffusive gas transfer, coupled with dissolution into the reaction medium resulted in irreproducible ^{34}S depletion of up to −6.3‰. Cryogenic transfer using liquid N_2 was slow and compromised the gas-tight seal on the manifold. Although gas transfer was quantitative, the risk of introducing O_2 was unacceptable. Fast, reproducible transfer was achieved by pumping the reaction vessel to vacuum and opening a valve to an H_2S-filled syringe. The H_2S was pulled quickly into the reaction vessel and the balance was made up using N_2. Gas transfer by this means took less than 10 s. The transferred H_2S from a gas bottle source had an isotopic composition of +15.4±0.3‰ and the transferred H_2S produced by acid $Na_2S \cdot 9H_2O$ decomposition had a composition of +4.9±0.6‰.

2.3. Extraction of products and analysis

Solid products were recovered by filtration on a 0.45-μm membrane filter and washed with N_2-purged 18 MΩ cm water before freeze drying. For isotopic analysis, S was extracted using acid $Cr(II)Cl_2$ decomposition, the evolved gas collected as ZnS, and converted to Ag_2S, washed with concentrated NH_3 and filtered and freeze-dried.

Reaction products were confirmed by powder X-ray diffraction. Freeze-dried samples were packed into aluminium powder holders and analysed using CoKα radiation on a Phillips PW1840 diffractometer.

Sulfur isotope ratios were analysed by combustion isotope ratio monitoring mass spectrometry (C-irmMS) [34]. Solids were weighed into Sn cups, mixed with V_2O_5 and combusted to SO_2 in an elemental analyzer coupled to a gas mass spectrometer via a gas mixing interface. Samples were analysed as Ag_2S except for S° and Na_2S_4, which were directly used for flash combustion. Most stable isotope measurements were carried out using a Carlo Erba EA 1108 elemental analyzer connected to a Finnigan MAT 252 gas isotope mass spectrometer via a MAT Finnigan Conflo II split interface (at ICBM Oldenburg). Additional samples were analyzed using a Finnigan Delta+ mass spectrometer coupled to a EuroVector elemental analyzer via a Finnigan Conflo II interface (at MPI-MM Bremen) or a Finnigan Delta S mass spectrometer coupled to a Carlo Erba EA via a Finnigan Conflo I interface (at UFZ Leipzig Halle). Cross-calibration of data sets was done via intercomparison materials. The isotopic composition is given

Table 1
FeS+H_2S: reaction conditions and products[a]

Exp. #	S(-II) source	$\delta^{34}S$ (‰ H_2S)	$\delta^{34}S$ (‰ FeS)	$\delta^{34}S$ (‰ FeS_2)	Mmol H_2S	Mmol FeS	Temp. (°C)
ISO1/120	H_2S	15.4	4.8	12.0	4.5	1.1	120
ISO2/120	H_2S	15.4	4.8	11.9	4.5	1.2	120
ISO3/120	$Na_2S \cdot 9H_2O$	4.9	12.5	6.2	4.5	1.2	120
ISO9/100	H_2S	15.4	4.8	11.9	4.5	1.2	100
ISO10/100	H_2S	15.4	4.8	11.5	4.5	1.1	100
ISO11/100	$Na_2S \cdot 9H_2O$	4.9	12.5	6.4	4.5	1.2	100
ISO12/100	$Na_2S \cdot 9H_2O$	4.9	12.5	7.4	4.5	1.2	100
ISO17/80	H_2S	15.4	4.8	13.3	4.5	1.1	80
ISO18/80	H_2S	15.4	4.8	12.7	4.5	1.2	80
ISO19/80	$Na_2S \cdot 9H_2O$	4.9	12.5	7.1	4.6	1.1	80
ISO20/80	$Na_2S \cdot 9H_2O$	4.9	12.5	7.4	4.6	1.2	80

[a] For all runs, total aqueous reaction volume was 11 ml. The Eh of each reaction was initially poised to <−400 mV using 1 ml of Ti(III) citrate. Reaction pH was maintained using pH 6 Hydrion™ buffer. Duration was 144 h.

in the δ-notation relative to the Vienna-Canõn Diablo Troilite (V-CDT) standard:

$$\delta^{34}S[‰] = \left\{ \left({}^{34}S/{}^{32}S_{sample} \right) / \left({}^{34}S/{}^{32}S_{V\text{–}CDT} \right) - \right\}.1000. \quad (5)$$

International standards (IAEA-S-1, IAEA-S-2, IAEA-S-3, IAEA-S-4, NBS-123, NBS-127) and in-house standards were used for mass-spectrometric calibration. Analytical reproducibility was ±0.2‰ (1σ) for MAT252 and Delta S and ±0.4‰ for Delta+ measurements, respectively.

The isotopic composition of potential reaction products were predicted via a binary isotope mixing equation using the measured δ-values of the respective end-members. This approach causes only minor uncertainty in the calculated isotope results. As an example, using typical end-member values of +5.00‰ and +15.00‰ (Tables 1–3), a mixing equation with δ-values yields +10.00‰. Considering the $^{32}S/^{34}S$ ratio of the V-CDT standard [35], a mass balance based on at.% leads to a numerical result of +9.98‰. The difference between the two values of 0.02‰ can be

Table 2
FeS+S_4^{2-}: reaction conditions and products[a]

Exp. #	$\delta^{34}S$ (‰ S_4^{2-})	$\delta^{34}S$ (‰ FeS)	$\delta^{34}S$ (‰ FeS_2)	Mmol S_4^{2-}	Mmol FeS	Temp. (°C)	Time (h)
ISO/Poly/1	12.1	6.0	11.2	3.5	3.4	100	216
ISO/Poly/2	12.1	6.0	11.6	6.9	3.4	100	216
ISO/Poly/3	12.1	6.0	11.5	4.6	3.4	100	216
$FeSS_4$/100/D	13.0	6.0	13.3	4.9	1.1	100	120
$FeSS_4$/100/E	13.0	6.0	13.0	5.2	1.3	100	120
$FeSS_4$/100/F	13.0	6.0	12.8	5.2	1.1	100	120
ISO5/120	13.3	4.8	12.2	5.1	1.2	120	168
ISO6/120	13.3	4.8	12.2	5.0	1.1	120	168
ISO7/120	13.3	12.5	12.6	5.0	1.2	120	168
ISO8/120	13.3	12.5	12.8	5.1	1.2	120	168
ISO13/100	13.3	4.8	12.2	5.0	1.1	100	144
ISO14/100	13.3	4.8	12.3	5.0	1.2	100	144
ISO15/100	13.3	12.5	12.9	5.0	1.1	100	144
ISO16/100	13.3	12.5	13.0	5.0	1.2	100	144

[a] For all reaction runs, total aqueous volume was 21 ml. A total of 1 ml of Ti(III) citrate was used to poise the Eh at a reducing value. Reaction pH was maintained at 12 by the excess of Na_2S_4 present. pH 8 buffer was used to ensure that an alkaline pH was maintained for experiments where Na_2S_4 was limited.

Table 3
Tetrasulfide experiments at 25 °C

Exp. #	$\delta^{34}S$ (‰ S_4^{2-})	$\delta^{34}S$ (‰ FeS)	$\delta^{34}S$ (‰ product)	Mmol S_4^{2-}	Mmol FeS	Temp. (°C)	Time (h)
FeSS4/25A	12.1	6.0	8.9	5	1.4	25	120
FeSS4/25B	12.1	6.0	9.9	5	1.3	25	120
FeSS4/25C	12.1	6.0	9.3	5	1.3	25	120

regarded as an upper limit and is considerably smaller than the typical precision of sulfur isotope measurements and the differences of isotope values discussed in the present study.

3. Results

Pyrite was formed in all experiments carried out between 80 and 120 °C. The detailed conditions and results for FeS/H_2S experiments and FeS/tetrasulfide experiments are shown in Tables 1 and 2, respectively. Powder XRD patterns for typical iron sulfide reactant and reaction products are illustrated in Fig. 1. Isotopic mixing lines showing reactant and FeS_2 compositions and calculated isotopic mixtures are illustrated for FeS/H_2S and FeS/tetrasulfide experiments in Figs. 2 and 3, respectively. Calculated isotopic mixtures use two approaches. In the first case, we assume that one unit of FeS reacts with one unit of H_2S or S_4^{2-} and that there is no isotopic exchange between the reservoirs prior to reaction to form pyrite. This mixture of two compounds is the mean of the reactant compositions:

$$\delta^{34}S_{FeS2} = \left(\delta^{34}S_{FeS} + \delta^{34}S_{H2S/S42-}\right)/2. \quad (6)$$

In the second approach, the isotopic composition of pyrite is the mean of the reactant compositions modified by the molar proportions of the reactants.

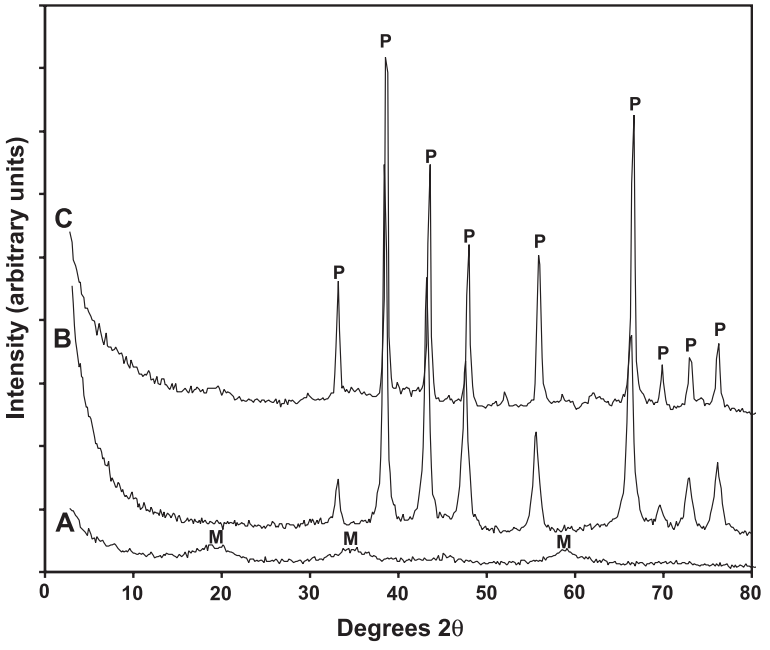

Fig. 1. Powder XRD data for typical FeS reactants and reaction products (CoKα radiation). Patterns are displaced vertically for clarity. FeS (pattern A) shows broad, weak Bragg reflections consistent with nanoparticulate mackinawite [19]. Pattern B illustrates the product of experimental run ISO/Poly/2 (Table 2) in which FeS was reacted with tetrasulfide. The product identifiable by XRD is exclusively pyrite. Pattern C illustrates the product of experimental run ISO1/120 (Table 1) in which FeS was reacted with H_2S. The product is almost entirely pyrite, although there is a suggestion of the basal reflection of mackinawite at 5 Å (~19° 2θ) indicating a small quantity of residual FeS.

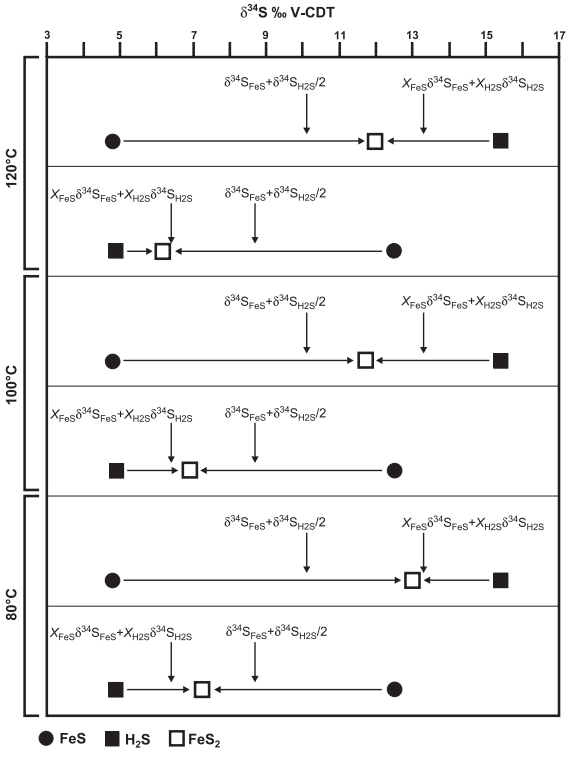

Fig. 2. Isotopic mixing lines for reactions using FeS and H_2S reactants. Reactant reservoirs are shown as filled circles (FeS) and filled squares (H_2S). Product pyrite is an open square. The position of the two simple isotopic mixtures on the mixing line is also shown. In all experiments, the composition of the pyrite product is intermediate between the two simple mixing models or is coincident with the complete isotopic mixture.

This represents the case where complete isotopic exchange between the reactants has occurred before pyrite formation:

$$\delta^{34}S_{FeS2} = x_{FeS}\delta^{34}S_{FeS} + x_{H2S/S42}\delta^{34}S_{H2S/S42-} \quad (7)$$

where x is the mole fraction of the component.

For all FeS/H_2S experiments, the isotopic composition of the pyrite falls either between that of the two calculated mixtures, or is equal to that of the mixture defined by Eq. (7) (Fig. 2). There is no temperature effect observable within the experimental range.

For FeS/S_4 experiments, the isotopic compositions of reactants where FeS was ^{34}S enriched over S_4^{2-} are too close to resolve mixing trends within experimental and analytical error. For other experiments, tetrasulfide is ^{34}S enriched over FeS by 6–8.5‰. The pyrite product is ^{34}S enriched over that resulting from either isotopic mixing model. The pyrite is ^{34}S depleted relative to the tetrasulfide reactant by 0–1‰.

A limited number of experiments were performed at 25 °C using tetrasulfide (Table 3). In these experiments, pyrite formation was expected to be slow, and isotope exchange between FeS

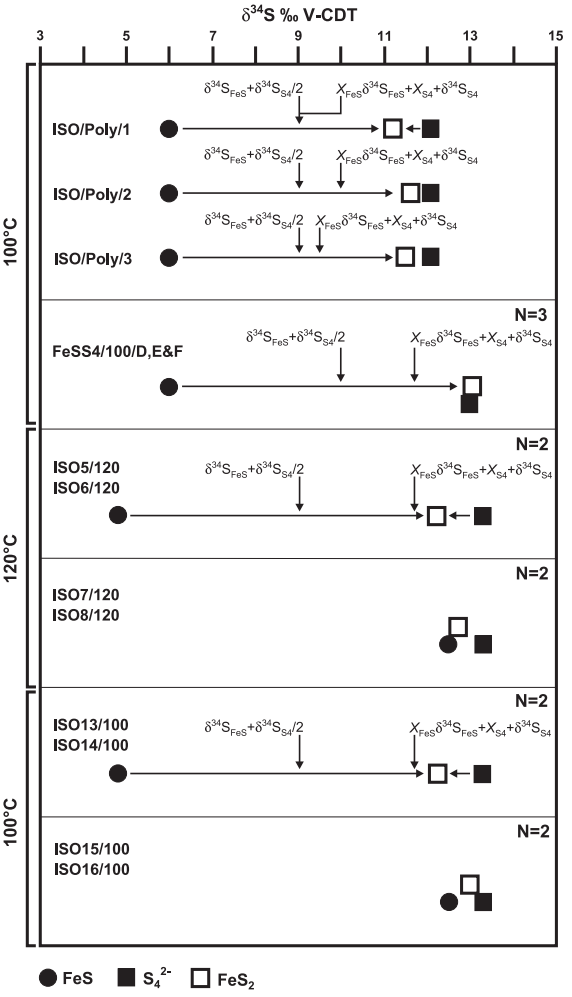

Fig. 3. Isotopic mixing lines for reactions using FeS and S_4^{2-} reactants. Reactant reservoirs are shown as filled circles (FeS) and filled squares (H_2S). Product pyrite is shown as an open square. The position of the two simple isotopic mixtures on the mixing line is also shown. In all experiments, the composition of the product pyrite is shifted towards the S_4^{2-} reservoir. Clear resolution of the trend is only possible for experiments where S_4^{2-} is ^{34}S enriched over FeS and, in these experiments, pyrite is ^{34}S enriched over both calculated isotopic mixtures, and is ^{34}S depleted relative to S_4^{2-} by <1‰.

and S_4^{2-} would be significant. The product of these reactions was quantitatively soluble in 6 N HCl and little or no pyrite was formed after 120 h. The composition of a binary isotope mixture as defined by Eq. (6) is +9‰ and that defined by Eq. (7) is +10.8‰. The non-pyritic products were ^{34}S depleted relative to the predicted values of +8.4±0.5‰.

4. Discussion

Published mechanisms for the polysulfide and H_2S pathways can be used to predict the pyrite isotopic composition and the outcome compared to experimental results. This provides an independent test of the proposed reaction mechanisms.

4.1. The H_2S pathway

The metastable persistence of FeS with H_2S is well known [30,36]. The pyrite nucleation barrier must be overcome for bulk formation of FeS_2 [37], since pyrite formation on a suitable substrate with only FeS and H_2S is fast [38]. Such substrates are reaction initiators and may include partially oxidized FeS [30], greigite (Fe_3S_4), sulfur grains, bacterial cell walls [39] or pyrite [38].

The kinetics and mechanism of the H_2S oxidation of FeS were determined by Rickard [22] and Rickard and Luther [23]. Textural observations, voltammetric measurements and an Arrhenius activation energy characteristic of transport control all point to the involvement of an $FeS_{(aq)}$ cluster complex (Fig. 4A) [23,40]:

$FeS_{(s)} = FeS_{(aq)}$	(fast < ca.100ºC > slow)	(8)
$FeS_{(aq)} + H_2S_{(aq)} = \{FeS\text{-}SH_2\}$	(fast)	(9)
$\{FeS\text{-}SH_2\} = [FeS_2.H_{2(occluded)}]$	(fast)	(10)
$[FeS_2.H_{2(occluded)}] = FeS_{2(s)} + H_{2(g)}$	(slow < ca.100ºC > fast)	(11)
$FeS_{(s)} + H_2S_{(aq)} = FeS_{2(s)} + H_{2(g)}$	Net reaction	(12)

The involvement of $FeS_{(aq)}$ and $H_2S_{(aq)}$ permits the development of coarse pyrite textures from nanoparticulate FeS [19,23].

In the H_2S pathway, sulfur in the product pyrite is the mean of the FeS and H_2S reservoirs. In the absence of other isotopic exchange or transfer processes, pyrite will inherit an isotopic composition reflecting equimolar mixing of the reservoirs.

The synthetic pyrite shows input from both the H_2S and FeS reservoirs (Table 1, Fig. 2). However, the result is more complex than that expected from 1:1 mixing and the pyrite shows a higher content of H_2S-sulfur than predicted. The data are consistent with mixing of the FeS and H_2S reservoirs by a process other than pyrite formation, and in one case (ISO3/120) the pyrite composition is consistent with complete isotopic mixing of the reactant reservoirs. In most cases, the pyrite composition is intermediate between those defined by the end-member models. Our results are consistent with two parallel exchange and reaction processes. Isotopic exchange occurs via solubility driven processes according to:

$Fe^{32}S + 2H^+ = Fe^{2+} + H_2{}^{32}S$		(13)
$Fe^{2+} + H_2{}^{34}S = Fe^{34}S + 2H^+$		(14)
$Fe^{32}S + H_2{}^{34}S = Fe^{34}S + H_2{}^{32}S$	Net exchange	(15)

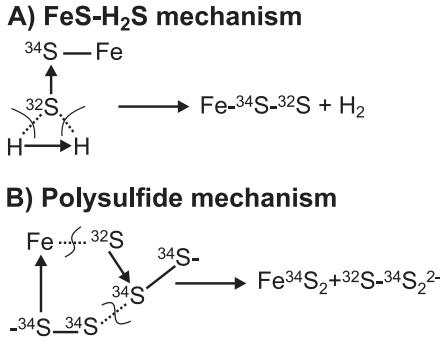

Fig. 4. Proposed reaction mechanisms for the formation of pyrite by (A) the reaction of FeS with polysulfide and (B) the reaction of FeS with H_2S. In both cases, an aqueous FeS cluster complex is the reactant. The polysulfide mechanism [20,21] proceeds via a cyclic intermediate. Cleavage of the Fe–S bond and the median S–S bond in S_4^{2-}, and formation of a bond between Fe and the S_2^{2-} so formed is expected to cause complete replacement of sulfur attached to Fe. The H_2S mechanism [23], by contrast, involves the oxidation of FeS by H_2S and sulfur is contributed to the product pyrite from both reactants.

Solubility driven isotopic mixing will occur readily at pH 6 and in the absence of pyrite formation the isotopic composition of all reactant S reservoirs asymptote towards the composition defined by Eq. (7). The experimentally observed and theoretical equilibrium sulfur isotope fractionation between FeS and aqueous H_2S is small at ambient temperatures [15,41] and insignificant at the temperatures used in this study.

Compared to FeS, FeS_2 is extremely sparingly soluble. Once fixed as pyrite, there is little or no opportunity for solubility driven isotope exchange. The isotopic composition of pyrite reflects 1:1 mixing of the two reactant reservoirs:

$$Fe^{32}S + H_2^{34}S = Fe^{32}S^{34}S + H_2 \quad (16)$$

where Eq. (16) is similar to Eq. (12). The isotopic composition of the synthetic pyrite will change as the experiment progresses and the composition of the two reactant reservoirs is modified by solubility exchange. Thus, the pyrite composition falls between that of the two boundary models. The relative rate of the processes defines the position of the pyrite on the isotopic mixing line in our experiments. Where solubility exchange is fast compared to fixation the pyrite is shifted towards the composition defined by Eq. (7).

4.2. The polysulfide pathway

The mechanism involves FeS dissolution and reaction with polysulfide to precipitate pyrite [21]. Voltammetric evidence confirms the involvement of an aqueous Fe sulfide cluster and a cyclic reaction intermediate of the iron sulfide cluster and polysulfide (Fig. 4B) [22].

$$FeS_{(s)} = FeS_{(aq)} \quad (8)$$

$$FeS_{(aq)} + S_n^{2-}{}_{(aq)} = \{(FeS)S_n\}^{2-} \quad (17)$$

$$\{(FeS)S_n\}^{2-} = FeS_{2(s)} + S_{n-1}^{2-}{}_{(aq)} \quad (18)$$

$$FeS_{(s)} + S_n^{2-}{}_{(aq)} = FeS_{2(s)} + S_{n-1}^{2-}{}_{(aq)} \quad \text{Net reaction} \quad (19)$$

The net reaction is the apparent addition of zero-valent S from S_n^{2-} to FeS.

The outcome of the polysulfide pathway is the transfer of sulfide between the reacting FeS and polysulfide complexes forming pyrite containing S_2^{2-} derived entirely from polysulfide (Fig. 4B). In the absence of other isotopic transfer or exchange processes, the pyrite product will have an isotopic composition identical to that of the polysulfide.

Where the composition of the reactants was sufficiently distinct to be resolved the pyrite composition was within 1‰ of the tetrasulfide reactant. Tetrasulfide was ^{34}S enriched over FeS, and pyrite was ^{34}S enriched in ^{34}S over the outcome of both mixing models but slightly ^{34}S depleted compared to the tetrasulfide. This is consistent with published reaction mechanisms [21,22]. The slight ^{34}S depletion of the pyrite may indicate some isotopic exchange between the FeS and S_4^{2-} reservoirs. Furthermore, during pyrite formation, ^{34}S depleted sulfur from FeS modifies the polysulfide reservoir and later formed pyrite will be ^{34}S depleted compared to early formed pyrite. The extent of solubility exchange is limited, consistent with the low FeS solubility at pH values near 12–13. Once fixed as FeS_2 the low solubility of pyrite precludes further exchange reactions. The experimental results further indicate that isotope fractionation into pyrite is not influenced by kinetic isotope effects from selective cleavage of S–S bonds in the polysulfide molecule [42].

Limited isotope exchange between FeS and tetrasulfide is confirmed by experiments at 25 °C (Table 3). Isotopic exchange occurs between polysulfide and FeS in the absence of pyrite formation, but cannot account for the recorded shift in isotopic composition at higher temperatures.

4.3. Re-evaluation of previous experimental data

Stable isotopes were included in previous studies of pyrite formation and the results attributed to the reaction of FeS with S° [26] or selective Fe loss [29]. In addition to these studies the fractionation of sulfur isotopes during pyrite synthesis via goethite (FeOOH) sulfidization has been investigated [43]. We revisit these data and rationalize the results within the framework of known reaction mechanisms and the only two pyrite formation mechanisms for which stoichiometry has been established.

Sweeney and Kaplan [26] investigated the reaction FeS and S° slurries with restricted exposure to atmospheric oxygen, but in the absence of excess H_2S. They reacted ^{34}S-enriched FeS with an excess of ^{34}S-depleted S°. The pyrite product showed a $\delta^{34}S$ composition intermediate between that of the S(-II) and S° end-members. In the absence of H_2S, isotope exchange between FeS and S° proceeds slowly [44]. The reaction of FeS phases (mackinawite or hexagonal pyrrhotite) with S° to produce pyrite via a greigite (Fe_3S_4) intermediate was proposed [26]. A probable mechanism is addition of S° to FeS via polysulfide [28]. In the present study, polysulfide reactions produce pyrite with $\delta^{34}S$ compositions close to that of the reactant tetrasulfide. In Sweeney and Kaplan's experimentation [26], the absence of excess H_2S means that polysulfide must be produced by the reaction of H_2S from FeS dissolution with S°. The reactant balance is represented by the dissolution of FeS, reaction of S(-II) with S° to produce polysulfide followed by pyrite formation:

$$FeS_{(s)} + 2H^+_{(aq)} = Fe^{2+}_{(aq)} + H_2S_{(aq)} \quad (20)$$

$$H_2S_{(aq)} + nS^o_{(s)} = S_{n+1}{}^{2-}_{(aq)} + 2H^+_{(aq)} \quad (21)$$

$$FeS_{(s)} + S_{n+1}{}^{2-}_{(aq)} = FeS_{2(s)} + S_n{}^{2-}_{(aq)} \quad (22)$$

$$Fe^{2+}_{(aq)} + S_n{}^{2-}_{(aq)} = FeS_{(s)} + n\text{-}1S^o_{(s)} \quad (23)$$

$$FeS_{(s)} + nS^o_{(s)} = FeS_{2(s)} + n\text{-}1S^o_{(s)} \quad \text{Net reaction} \quad (3)$$

This balance does not imply a specific mechanism, but illustrates that the net stoichiometry by this reaction route is the apparent addition of S° to FeS, mediated via the polysulfide pathway since Eq. (22) is identical to Eq. (19). The reactant polysulfide is an isotopic mixture of the S(-II) and S° end-members and the product pyrite displays an sulfur isotope composition intermediate between that of the reactant FeS and S° phases, as reported by Sweeney and Kaplan [26].

Wilkin and Barnes [29] examined pyrite formation from FeS and Fe_3S_4 reactants with reduced and partially oxidized sulfur sources. They introduced limited quantities of O_2 to their reactions, a similar but more controlled approach to that of Sweeney and Kaplan [26]. Their results show that within analytical precision, synthetic pyrite had an identical sulfur isotopic composition to that of the reacting educts FeS or Fe_3S_4. Wilkin and Barnes [29] concluded that pyrite formation may proceed, not by addition of S° to FeS, but by oxidative Fe loss:

$$2FeS_{(s)} + 2H^+_{(aq)} = FeS_{2(s)} + Fe^{2+}_{(aq)} + H_{2(g)}. \quad (4)$$

At first glance, it is difficult to reconcile these results with those of the present study. However, Eq. (4) is the sum of FeS dissolution (Eq. (20)) and subsequent reaction of FeS with H_2S (Eq. (12)):

$$FeS_{(s)} + 2H^+_{(aq)} = Fe^{2+}_{(aq)} + H_2S_{(aq)} \quad (20)$$

$$FeS_{(s)} + H_2S_{(aq)} = FeS_{2(s)} + H_{2(g)} \quad (12)$$

$$2FeS_{(s)} + 2H^+_{(aq)} = FeS_{2(s)} + Fe^{2+}_{(aq)} + H_{2(g)} \quad \text{Net reaction} \quad (4)$$

The net reaction postulated by Wilkin and Barnes [29] can be explained by a process akin to that postulated to explain the results of Sweeney and Kaplan's [26] observations. However, we must reconcile the observation that, while the pyrite product retained the FeS isotopic composition, there were other sulfur compounds with distinct isotopic signatures present, including S°, H_2S, $S_2O_3^{2-}$ and $S_4O_6^{2-}$.

We compare the rates of the polysulfide and H_2S pathways under the experimental conditions of Wilkin and Barnes [29] using known reaction kinetics [20,22]. Wilkin and Barnes [29] report that they used 100 mg of FeS and maintained an H_2S partial pressure of 0.03 atm in their experiments. Rickard [22] showed that:

$$dFeS_2/dt = k(FeS)(cH_2S) \quad (24)$$

where (FeS) is the molar concentration of FeS, cH_2S is the molar concentration of H_2S and k is the rate constant. For the temperatures used in the experimentation, k is of the order of 2×10^{-3} l mol^{-1} s^{-1} [22]. The initial pyrite formation rate is ~2×10^{-8} mol l^{-1} s^{-1} at pH 7, sufficient to ensure complete reaction of FeS to FeS_2 within 24–48 h. We assume that the surface areas of the reactants used by Wilkin and Barnes [29] and Rickard [22] are similar.

Where polysulfide was present, the reaction kinetics are summarized by:

$$dFeS_2/dt = k(FeS)^2(S)\left\{\sum S(-II)\right\}\{H+\} \quad (25)$$

where (FeS) and (S) are the FeS and S° surface areas in cm^2, $\{\sum S(-II)\}$ is the total dissolved sulfide activity and {H+} is the hydrogen ion activity [20]. The rate constant is of the order of 10^{-12} cm^6 mol^{-1} l^{-1} s^{-1} at 40 °C [20]. Values for the FeS surface area have been determined by various workers, and estimates include 16–21 [30], 44 [20], 7 [24] and 37 m^2 g^{-1} [22]. Therefore, we take 30 m^2 g^{-1} as a representative value. For precipitated S°, Rickard [20] reports a mean surface area of 1.4×10^3 cm^2 g^{-1}. If we consider comparable initial conditions to those discussed above for the H_2S pathway, and take the mass of S° to be equivalent to that of the FeS then for the polysulfide pathway at pH7 the estimated initial rate, $dFeS_2/dt$, is of the order of 8×10^{-11} mol l^{-1} s^{-1}. The initial rate of the H_2S pathway is 2 orders of magnitude greater than for the polysulfide pathway and at pH7 and millimolar total S(-II), the total equilibrium polysulfide concentration is $<10^{-4}$ M [45] and is rate limiting. Pyrite formation via the polysulfide pathway is too slow for ^{34}S enriched polysulfide to contribute to the isotopic composition of pyrite. Other oxidized sulfur species were present in some experiments but there is no published evidence for their direct involvement in pyrite formation.

In Wilkin and Barnes' experiments [29], the boundary conditions favour pyrite formation via the H_2S pathway. The $\delta^{34}S$ composition was 2.8‰ for sodium sulfide nonahydrate (used to prepare FeS) and 3.3‰ for H_2S [29].

Within analytical error, the two sulfide sources have identical isotopic compositions. The isotope results of Wilkin and Barnes [29] are consistent with pyrite formation by the reaction of FeS (δ^{34}S=2.8‰) and H_2S (δ^{34}S=3.3‰). The outcome is the same as that predicted for oxidative Fe loss from FeS (Eq. (4)). There is no need to invoke a novel mechanism of oxidative Fe loss for pyrite formation to explain the sulfur isotope data. Furthermore, the proposed Fe-loss pathway does not explain S_2^{2-} formation and Fe(II) spin state changes during pyrite formation. The experimental data of Wilkin and Barnes [29] indicate that the principal pyrite formation pathway in pH neutral environments is the H_2S pathway.

Price and Shieh [43] examined goethite sulfidization to pyrite using a 30-fold molar excess of H_2S at pH 4–5 and 22–24 °C. Early-formed FeS_2 was depleted in ^{34}S relative to H_2S, but after 65 days of reaction the pyrite was isotopically identical to the H_2S. The data suggest a small kinetic isotope fractionation on pyrite formation, but because a single buffered sulfur source was used, give little information concerning reaction pathway. At ambient temperatures, the sulfur isotope fractionation upon pyrite formation is small [43] and insignificant at elevated temperatures.

4.4. Sulfur isotope partitioning into sedimentary sulfides: a proxy for pyritization pathways?

Published kinetic investigations [20–23] demonstrate that the polysulfide and H_2S pathways remain mechanistically uniform from 5 to 125 °C. Therefore, it is possible to extrapolate our results to ambient natural systems as well as to medium-temperature hydrothermal systems.

Experimental conditions maximize reaction rates for the respective pathways. FeS–H_2S reactions were performed at pH6 where sulfide speciation is dominated by H_2S (pK_{1H2S}=6.98 [46]) and [$FeS_{(aq)}$] is not limited by acid dissociation. For the polysulfide pathway, an alkaline pH of 12–13 maximized S_n^{2-} activity [45] and made H_2S a minor species. Isotope fractionation between different dissolved sulfur species in the system H_2S–H_2O [15,41] does not influence the experimental results.

In ambient sediments, reactant concentrations are lower than in our experiments, and the pyrite formation rate is less. Luther et al. [47] report the results of voltammetric investigations of the aqueous sulfide speciation of marine, hydrothermal and fresh waters. This approach determines $H_2S/HS^-_{(aq)}$, $S^{2-}_{n(aq)}$ and $FeS_{(aq)}$ as discrete species [48–51]. Detectable polysulfide is present at the oxic/anoxic interface, but $H_2S/HS^-_{(aq)}$ and $FeS_{(aq)}$ dominate in reduced environments below the oxic/anoxic interface [47]. In-situ measurements of sulfide speciation and O_2 in hydrothermal vents reveal $H_2S/HS^-_{(aq)}$ concentrations of <50 μM in all the environments investigated, but where temperatures exceed 30 °C, appreciable $FeS_{(aq)}$ formation occurs [49]. Despite the presence of coexisting H_2S/HS^- and O_2, aqueous polysulfide is not observed immediately above hydrothermal vent chimneys [50] but is present where diffuse hydrothermal fluids mix with seawater [49].

Since aqueous H_2S and HS^- are the predominant forms of free sulfide below the oxic/anoxic interface, the dominant pyrite formation pathway in those environments is the H_2S reaction [47]. The polysulfide reaction, however, is important at the oxic/anoxic interface at pH>7.5 where H_2S becomes a minor free sulfide species [47]. Polysulfide may be generated on oxyhydroxide mineral surfaces (e.g. $Fe(OH)_3$, FeOOH) in sediments or within hydrothermal systems where sulfidic fluids, oxic seawater and mineral surfaces can interact. The extent of polysulfide formation is difficult to ascertain, but the absence of detectable polysulfide [47] indicates that, if produced, S_n^{2-} is quickly reacted before it appears as an aqueous component. The polysulfide pathway is important in the onset of pyrite formation. Further pyrite formation in the absence of polysulfide proceeds via the H_2S pathway.

Free sulfide speciation is dominated by H_2S/HS^- below the oxic/anoxic interface and consequently the H_2S pathway dominates pyrite formation in these environments. Consequently, the isotopic composition of pyrite might be used to determine the evolution of reactant reservoirs because the isotopic composition of pyrite reflects the composition of both reservoirs. The relative rate of sulfur isotope fixation in FeS_2 versus equilibration of FeS and H_2S will exert a major control on the composition of FeS_2. Where fixation as FeS_2 is very fast relative solubility

exchange then pyrite will tend towards a 1:1 mixture of the reactant reservoirs. If fixation as FeS_2 is sufficiently slow to permit isotopic equilibration of the reservoirs, then the pyrite composition will reflect the mean of the composition of the reservoirs.

We discuss how our experimental pyritization rates compare to those in nature. The rate constant for the H_2S pathway is 3×10^{-3} l mol^{-1} s^{-1} at 100 °C [22], the initial FeS concentration is ~1×10^{-1} mol l^{-1} and the initial H_2S is ~1×10^{-1} mol l^{-1}, and so initial $dFeS_2/dt$ is of the order of 2 mol l^{-1} day^{-1} in our experiments. The range of calculated pyrite formation rates for ambient sediments is 10^{-17}–10^{-12} mol l^{-1} day^{-1} [22]. The pyrite formation rate in hydrothermal systems will be intermediate between these extreme values. Isotopic equilibration of FeS with H_2S is fast [44] and in natural sedimentary and hydrothermal environments pyrite formation is sufficiently slow to permit local isotopic equilibration of FeS and H_2S reservoirs. In our experiments, initial pyrite formation rates are 12–17 orders of magnitude greater than those calculated for sediments and it is possible to discern the effect of the pyrite formation pathway on the isotopic composition of synthetic pyrite.

We have considered only inorganic processes. Iron sulfide formation during bacterial disproportionation of elemental sulfur shows isotopic evidence for pyrite formation by the reaction of polysulfide and H_2S with FeS [9]. In experiments conducted by Canfield et al. [9], the pyritization reactions proceeded with similar rates and up to 100,000 times faster than expected from inorganic kinetics. Pyrite formation associated with these bacterial processes will be significant close to the oxic/anoxic boundary in sediments [9]. The influence of bacterial processes in the anoxic zones remains a largely unknown factor. Donald and Southam [39] examined low temperature anaerobic bacterial transformation of FeS to pyrite and compared the outcome to abiotic processes. They found the bacterially mediated process to be more efficient at converting FeS to FeS_2. A number of factors were important including the role of the bacterial cell wall and the release of bacterial organic sulfur products [39]. The relative contributions of abiotic reactions and bacterially mediated reactions to sedimentary and hydrothermal pyrite formation rates remains unknown and the role of bacteria requires further experimental and field investigations.

We anticipate that isotopic analysis of pyrite forming reactants and products in natural systems to be fraught with difficulties when using simplified analytical schemes. Morse and Rickard [52] re-evaluated the operational definition of acid volatile sulfide (AVS) for sediments, which is typically extracted anoxically using 6M HCl [53]. AVS is a complex and variable mixture of dissolved species and clusters (H_2S, HS^-, $FeS_{(aq)}$ and partially S_n^{2-}) and mineral phases (FeS, mackinawite and partially greigite) [52–54]. Care must be taken in the chemical and isotopic analysis of sedimentary AVS because it is subject to the relative proportions of aqueous and mineral components and to the method used for extraction [52–56]. Only sophisticated extraction methods can be used to characterize the different reservoirs involved in sedimentary pyrite formation [52,55,56].

Further difficulties arise from the H_2S mechanism. Reactants are aqueous species [23] and transport considerations mean that pyrite formation need not be related to AVS distribution spatially or temporally [52,57]. Depth analyses of AVS and pyrite in modern steady-state sedimentary sequences typically show decreasing AVS and increasing pyrite with depth. An interpretation commonly applied is that FeS, attributed to AVS, converts to pyrite with depth. The mass balance for this process, however, does not add up when applied to the observed AVS-pyrite plots [57]. Sulfur isotopic studies, which characterize the depth profiles for the isotopic composition of AVS and Cr(II) reducible sulfur (CRS), often attributable to pyrite, reveal that AVS compositions sometimes shadow CRS compositions, e.g. [58], but AVS and CRS trends may also be locally divergent. e.g. [55,59]. If CRS is a bulk isotopic reservoir representing sulfur fixed as pyrite throughout the history of the sediment and AVS represents mobile aqueous reactants with the capacity for rapid isotopic exchange [44], then we find no a priori reason to suppose that AVS isotopic signatures should be directly related to the bulk solid phase CRS signatures with which they coexist at the time of sampling. Further detailed work is needed to resolve the potential of stable sulfur isotope signatures to extract mechanistic information for sedimentary pyrite forming pathways.

5. Conclusions

The results of this and previously published isotopic studies are consistent with proposed reaction mechanisms for pyrite formation based on the polysulfide [20,21] and H_2S [22,23] pathways. Our results are an experimentally independent verification of the reaction mechanisms. The polysulfide pathway permits exchange of sulfur from the polysulfide during pyrite formation and newly formed pyrite inherits the polysulfide isotopic composition. The H_2S pathway forms pyrite, the isotopic composition of which reflects the composition of both FeS and H_2S reservoirs. Experimental conditions were optimized to enhance pyrite formation rates by the respective mechanisms; however, even with rapid fixation as pyrite, evidence of isotopic exchange via solubility processes was evident and these modify the pyrite isotopic composition slightly from the ideal composition predicted from the reaction mechanisms. The extent of this is controlled by the relative fixation versus exchange rates.

Previous experimental studies using stable isotope partitioning [26,29] are shown to be consistent with the H_2S and polysulfide pathways. There is, as yet, no compelling evidence to invoke the activity of other notional reaction pathways for pyrite formation, either in the laboratory or in ambient aqueous natural systems. However, evidence from microbiological experiments [9,39] points to enhanced pyrite formation rates compared to abiotic processes. It remains to be seen if the increase in pyrite formation rate is due to bacterial catalysis of known pathways or the involvement of previously unsuspected reactions.

Voltammetric measurements of natural aqueous FeS and sulfide speciation [47–51] combined with kinetic considerations indicate that the H_2S pathway will dominate in most environments. Experimental initial pyrite formation rates are 12–17 orders of magnitude greater than those calculated for sediments [22] yet partial isotopic equilibration of FeS and H_2S is evident, and isotope exchange between FeS and H_2S will be significant in natural systems. The influence of the H_2S mechanism on pyrite isotopic composition is unlikely to be a significant control on the composition of natural pyrite. We conclude that the sulfur isotopic composition of pyrite normally reflects the average composition of the sulfide reservoir from which it was formed. This means that the isotope compositions of pyrite sulfur and variations in ancient systems can be used to help determine the evolution of the biogeochemical sulfur cycle and the development of related biogeochemical cycles through time.

Acknowledgements

This work was supported by NERC grant GR3/11376 to DR, a Leverhulme Special Research Fellowship (SRF/2000/246) to IBB and Max Planck Society to MEB. MEB also wishes to thank J. Rullkötter for the allowance to use the mass spectrometer at the ICBM (University of Oldenburg) and M. Gehre (UFZ Leipzig-Halle) for supporting measurements. Additionally, the authors would like to thank A. Boyce (SUERC) for his contribution to confirm the isotopic composition of tetrasulfide. G.W. Luther III and J.W. Morse are thanked for constructive reviews of the original manuscript.

References

[1] R. Raiswell, Pyrite texture, isotopic composition and the availability of iron, Am. J. Sci. 282 (1982) 1244–1263.
[2] H. Ohmoto, C.J. Kaiser, K.A. Geer, Systematics of sulfur isotopes in recent marine sediments and ancient sediment-hosted base metal deposits, in: H.K. Herbert, S.E. Ho (Eds.), Stable isotopes and fluid processes in mineralization, The University of Western Australia Publication, vol. 23, 1990, pp. 70–120.
[3] H. Strauss, The isotopic composition of sedimentary sulfur through time, Palaeogeogr. Palaeoclimatol. Palaeoecol. 132 (1997) 97–118.
[4] H.F. Passier, J.J. Middelburg, G.J. de Lange, M.E. Böttcher, Modes of sapropel formation in the eastern Mediterranean: some constraints based on pyrite properties, Mar. Geol. 153 (1999) 199–219.
[5] N. Nakai, M.L. Jensen, The kinetic isotope effect in the bacterial reduction and oxidation of sulfur, Geochim. Cosmochim. Acta 28 (1964) 1893–1912.
[6] L.A. Chambers, P.A. Trudinger, J.W. Smith, M.S. Burns, Fractionation of sulfur isotopes by continuous cultures of *Desulfovibrio desulfuricans*, Can. J. Microbiol. 21 (1975) 1602–1607.
[7] D.E. Canfield, Isotope fractionation by natural populations of sulfate-reducing bacteria, Geochim. Cosmochim. Acta 65 (2001) 1117–1124.
[8] B. Fry, J. Cox, H. Gest, J.M. Hayes, Discrimination between ^{34}S and ^{32}S during bacterial metabolism of inorganic sulfur compounds, J. Bacteriol. 165 (1986) 328–330.

[9] D.E. Canfield, B. Thamdrup, S. Fleischer, Isotope fractionation and sulfur metabolism by pure and enrichment cultures of elemental sulfur disproportionating bacteria, Limnol. Oceanogr. 43 (1998) 253–264.
[10] H. Cypionka, A.M. Smock, M.E. Böttcher, A combined pathway of sulfur compound disproportionation in *Desulfovibrio desulfuricans*, FEMS Microbiol. Lett. 166 (1998) 181–186.
[11] K. Habicht, D.E. Canfield, J. Rethmeier, Sulfur isotope fractionation during bacterial reduction and disproportionation of thiosulfate and sulfite, Geochim. Cosmochim. Acta 62 (1998) 2585–2595.
[12] M.E. Böttcher, B. Thamdrup, T.W. Vennemann, Oxygen and sulfur isotope fractionation during anaerobic bacterial disproportionation of elemental sulfur, Geochim. Cosmochim. Acta 65 (2001) 1601–1609.
[13] R. Knott, A.E. Fallick, D. Rickard, H. Backer, Mineralogy and sulfur isotope characteristics of a massive sulfide boulder, Galapagos Rift, 85°55′W, in: L.M. Parson, C.L. Walker, D.R. Dixon (Eds.), Hydrothermal Vents and Processes, Geol. Soc. London Spec. Pub. 87 (1995) 207–222.
[14] R. Saez, G.R. Almodovar, E. Pascual, Geological constraints on massive sulfide genesis in the Iberian pyrite belt, Ore Geol. Rev. 11 (1996) 429–451.
[15] H. Ohmoto, M.B. Goldhaber, Sulfur and carbon isotopes, in: H.L. Barnes (Ed.), Geochemistry of Hydrothermal Ore Deposits, John Wiley & Sons, London, 1997, pp. 517–611.
[16] H. Sakai, D.J. Des Marais, A. Ueda, J. Moore, Concentrations and isotope ratios of C, N and S in ocean floor basalts, Geochim. Cosmochim. Acta 48 (1984) 2433–2441.
[17] C.E. Rees, W.J. Jenkins, J. Monster, The sulfur isotopic composition of ocean water sulfate, Geochim. Cosmochim. Acta 42 (1978) 377–382.
[18] M.E. Böttcher, H.J. Brumsack, C.D. Dürselen, B.B. Jørgensen, The isotopic composition of dissolved sulfate in the modern ocean, marginal seas and anoxic basins, Beih. Eur. J. Mineral. 15 (2003) 26.
[19] M. Wolthers, S.J. van der Gaast, L. Charlet, D. Rickard, A surface and structural model describing the environmental reactivity of disordered mackinawite, Am. Mineral. 88 (2004) 2007–2015.
[20] D. Rickard, Kinetics and mechanism of pyrite formation at low temperatures, Am. J. Sci. 275 (1975) 636–652.
[21] G.W. Luther III, Pyrite synthesis via polysulfide compounds, Geochim. Cosmochim. Acta 55 (1991) 2839–2849.
[22] D. Rickard, Kinetics of pyrite formation by the H2S oxidation of iron(II) monosulfide in aqueous solutions between 25 °C and 125 °C: the rate equation, Geochim. Cosmochim. Acta 61 (1997) 115–134.
[23] D. Rickard, G.W. Luther III, Kinetics of pyrite formation by the H_2S oxidation of iron(II) monosulfide in aqueous solutions between 25 °C and 125 °C: the mechanism, Geochim. Cosmochim. Acta 61 (1997) 135–147.
[24] P. Taylor, T.E. Rummery, D.G. Owen, Reactions of iron monosulfide solids with aqueous hydrogen sulfide up to 160 °C, J. Inorg. Nucl. Chem. 41 (1979) 1683–1687.
[25] E. Drobner, H. Hubner, G. Wächterhauser, D. Rose, K.O. Setter, Pyrite formation linked with hydrogen evolution under anaerobic conditions, Nature 346 (1990) 742–744.
[26] R.E. Sweeney, I.R. Kaplan, Pyrite framboid formation: laboratory synthesis and marine sediments, Econ. Geol. 68 (1973) 618–634.
[27] R.A. Berner, Sedimentary pyrite formation, Am. J. Sci. 268 (1970) 1–23.
[28] M.A.A. Schoonen, H.L. Barnes, Reactions forming pyrite and marcasite from solution: II via FeS precursors below 100 °C, Geochim. Cosmochim. Acta 60 (1991) 115–134.
[29] R.T. Wilkin, H.L. Barnes, Pyrite formation by reactions of iron monosulfides with dissolved inorganic and organic sulfur species, Geochim. Cosmochim. Acta 60 (1996) 41267–44179.
[30] L.G. Benning, R.T. Wilkin, H.L. Barnes, Reaction pathways in the Fe–S system below 100 °C, Chem. Geol. 167 (2000) 25–51.
[31] I.B. Butler, M.A.A. Schoonen, D. Rickard, Removal of dissolved oxygen from water: a comparison of four common techniques, Talanta 41 (1994) 211–215.
[32] E. Rosen, R. Tegman, Preparative and X-ray powder diffraction study of the polysulfides Na_2S_2 and Na_2S_4 and Na_2S_5, Acta Chem. Scand. 25 (1971) 3329–3336.
[33] A.J.B. Zehnder, K. Wuhrmann, Ti(III) citrate as a nontoxic oxidation–reduction buffering system for the culture of obligate anaerobes, Science 192 (1976) 1165–1167.
[34] M.E. Böttcher, B. Schnetger, Direct measurement of the content and isotopic composition of sulfur in black shales by means of combustion-isotope-ratio-monitoring mass spectrometry (C-irmMS), in: P. de Groot (Ed.), Handbook of Stable Isotope Analytical Techniques, Elsevier, Amsterdam, 2004, pp. 597–603.
[35] T. Ding, S. Valkiers, H. Kipphardt, P. Bièvre, P.D.P. Taylor, H. Krouse, Calibrated sulfur isotope abundance ratios of three IAEA sulfur isotope reference materials and V-CDT with a reassessment of the atomic weight of sulfur, Geochim. Cosmochim. Acta 65 (2001) 2433–2437.
[36] D. Rickard, The chemistry of iron sulfide formation at low temperatures, Stockholm Contrib. Geol. 20 (1969) 67–95.
[37] I.B. Butler, D. Rickard, S.T. Grimes, A. Oldroyd, Nucleation and growth of pyrite on pyrite seeds, Abstr. Pap. Am. Chem. Soc., 2003, GEOC 11, ISBN 0-8412-3873-1.
[38] N.G. Harmandas, E. Navarro Fernadez, P.G. Koutsoukos, Crystal growth of pyrite in aqueous solutions. Inhibition by organophosphorous compounds, Langmuir 14 (1998) 1250–1255.
[39] R. Donald, G. Southam, Low temperature anaerobic bacterial diagenesis of ferrous monosulfide to pyrite, Geochim. Cosmochim. Acta 63 (1999) 2019–2023.
[40] S. Theberge, G.W. Luther III, Determination of the electrochemical properties of a soluble aqueous FeS species present in sulfidic solution, Aquat. Geochem. 3 (1997) 191–211.
[41] M.E. Böttcher, A.M. Smock, H. Cypionka, Sulfur isotope fractionation during experimental precipitation of iron(II) and manganese(II) sulfide at room temperature, Chem. Geol. 146 (1998) 127–134.

[42] H. Sakai, Sulfur isotope chemistry of polysulfide solution, J. Inorg. Nucl. Chem. 28 (1966) 1567–1573.
[43] F.T. Price, Y.N. Shieh, Fractionation of sulfur isotopes during laboratory synthesis of pyrite at low temperatures, Chem. Geol. 27 (1979) 245–253.
[44] H. Fossing, B.B. Jørgensen, Isotope exchange reactions with radiolabelled sulfur compounds in anoxic seawater, Biogeochemistry 9 (1990) 223–245.
[45] J. Boulegue, G. Michard, Constantes de formation des ions polysulfures S_6^{2-}, S_5^{2-} et S_4^{2-} en phase aquese, J. Fr. Hydrol. 9 (1978) 27–34.
[46] O.M. Suleimenov, T.M. Seward, A spectrophotometric study of hydrogen sulfide ionization in aqueous solutions to 350 °C, Geochim. Cosmochim. Acta 61 (1997) 5187–5198.
[47] G.W. Luther III, M. Taillfert, T.F. Rozan, D. Rickard, Geochemical implications of the polysulfide vs. sulfide pyrite formation reactions based on real time measurements of soluble reactants, Abstr. Pap. - Am. Chem. Soc., 2003, GEOC9, ISBN 0-8412-3873-1.
[48] T.F. Rozan, S. Theberge, G.W. Luther III, Quantifying elemental sulfur (S-0), bisulfide (HS^-) and polysulfide (S_{-x}^{2-}) using a voltammetric method, Anal. Chim. Acta 415 (2000) 175–184.
[49] G.W. Luther III, B.T. Glazer, L. Hohmann, J.I. Popp, M. Taillfert, T.F. Rozan, P.J. Brendel, S.T. Theberge, D.B. Nuzzio, Sulfur speciation monitored in-situ with solid state gold amalgam voltammetric microelectrodes: polysulfides as a special case in sediments, microbial mats and hydrothermal vent waters, J. Environ. Monit. 3 (2001) 61–66.
[50] G.W. Luther III, T.F. Rozan, M. Taillfert, D.B. Nuzzio, C. Di Meo, T.M. Shank, R.A. Lutz, S. Craig Cary, Chemical speciation drives hydrothermal vent ecology, Nature 410 (2001) 813–816.
[51] D. Rickard, A. Oldroyd, A. Cramp, Voltammetric evidence for soluble FeS complexes in anoxic estuarine muds, Estuaries 22 (1999) 639–701.
[52] J.W. Morse, D. Rickard, Chemical dynamics of sedimentary acid volatile sulfide (AVS): implications for metal toxicity, Environ. Sci. Technol. 38 (2004) 131A–136A.
[53] J.C. Cornwell, J.W. Morse, The characterization of iron sulfide minerals in anoxic marine sediments, Mar. Chem. 22 (1987) 193–206.
[54] N.N. Zhabina, I.I. Volkov, A method of determination of various sulfur compounds in sea sediments and rocks, in: W.E. Krumbein (Ed.), Environmental Biogeochemistry and Geomicrobiology—Methods, Metals, and Assessment, vol. 3, Ann Arbor Sci., 1978, pp. 735–746.
[55] B.B. Jørgensen, M.E. Böttcher, H. Lüschen, L.N. Neretin, I.I. Volkov, Isotopically heavy sulfides caused by anaerobic methane oxidation and a deep H_2S sink in Black Sea sediments, Geochim. Cosmochim. Acta 68 (2004) 2095–2118.
[56] L.N. Neretin, M.E. Böttcher, B.B. Jørgensen, I.I. Volkov, H. Lüschen, K. Hilgenfeldt, Pyritization processes and greigite formation in the advancing sulfidization front in the Upper Pleistocene sediments of the Black Sea, Geochim. Cosmochim. Acta 68 (2004) 2081–2093.
[57] D. Rickard, A. Oldroyd, The origin of pyrite-acid volatile sulfide (AVS) cross-over plots in sediment profiles, J. Conf. Abstr. 6 (1) (2001) 256.
[58] T.W. Lyons, Sulfur isotopic trends and pathways of iron sulfide formation in upper Holocene sediments of the anoxic Black Sea, Geochim. Cosmochim. Acta 61 (1997) 3367–3382.
[59] A.L. Bates, E.C. Spiker, C.W. Holmes, Speciation and isotopic composition of sedimentary sulfur in the Everglades, Florida, USA, Chem. Geol. 146 (1998) 155–170.